Gravitational waves from accretion disks: Turbulence, mode excitation, and prospects for future detectors

Chen Yuan[®], ^{1,*} Vitor Cardoso[®], ^{1,2} Francisco Duque[®], ³ and Ziri Younsi[®]

¹CENTRA, Departamento de Física, Instituto Superior Técnico—IST, Universidade de Lisboa—UL,

Avenida Rovisco Pais 1, 1049-001 Lisboa, Portugal

²Niels Bohr International Academy, Niels Bohr Institute, Blegdamsvej 17, 2100 Copenhagen, Denmark

³Max Planck Institute for Gravitational Physics (Albert Einstein Institute),

Am Mühlenberg 1, D-14476 Potsdam, Germany

⁴Mullard Space Science Laboratory, University College London,

Holmbury Saint Mary, Dorking, Surrey, RH5 6NT, United Kingdom

(Received 4 October 2024; revised 26 November 2024; accepted 11 February 2025; published 17 March 2025)

We study gravitational-wave emission by turbulent flows in accretion disks around spinning black holes or neutron stars. We aim to understand how turbulence can stochastically excite black hole quasinormal ringing and contribute to a stochastic gravitational-wave background from accretion disks around compact objects. We employ general relativistic magnetohydrodynamic simulations and feed them as the source of the Teukolsky master equation to evaluate the gravitational wave energy spectrum of a single source. The stochastic gravitational wave background from accretion disks generated by the population of stellar-mass compact objects is far below the sensitivity of third-generation ground-based detectors. In contrast, the supermassive black hole population, in particular those actively accreting, could lead to $\Omega_{\rm GW} \sim 10^{-15}$ in the microhertz. This signal remains well below the sensitivities of pulsar-timing arrays and LISA, making direct observation infeasible.

DOI: 10.1103/PhysRevD.111.063048

I. INTRODUCTION

The remarkable detection of gravitational waves (GWs) from the merger of two black holes (BHs) by the LIGO-Virgo Scientific collaboration [1,2] inaugurated a new era in physics [3–6]. The understanding of mechanisms for BH formation and growth across cosmic time [4,5], of possible phase transitions in the early Universe [7–14], or the nature of dark matter are now within reach [15–32]. Even more intriguing is the opportunity to test gravity in the strong-field regime, particularly near BH horizons. Of particular interest to us here are rotating BHs surrounded by an accretion disk.

Accretion disks are interesting probes of strong gravitational fields and of extreme astrophysical processes, where the role of BH rotation, surrounding plasma and magnetic fields is yet to be fully understood. The dynamics of accretion disks are incredibly complex and rich. Among others, one of the crucial factors is turbulence [33,34], which breaks the axial symmetry of the system and leads to the emission of light but also GWs, providing new avenues for understanding the behavior of accretion disks. In the same way that turbulence in the Sun drives the stochastic excitation of its characteristic modes [35–37], it might be

*Contact author: chenyuan@tecnico.ulisboa.pt

expected that turbulent accretion can excite modes of BHs, but a precise calculation has not been done. An order of magnitude estimate was attempted in the past [38], but missed all the intricate features of astrophysical disks. The formation mechanism of collapsar disks was recently studied [39], with the conclusion that the resulting GW emission could reach the sensitivities of current and future ground-based detectors. This—the possible stochastic excitation of quasinormal modes of BHs—was, in fact, our original motivation to understand GW emission from systems including a BH and an accretion disk.

The superposition of GW sources will form a stochastic GW background (SGWB). The study of the SGWB generated by accretion disks is instrumental in refining our theoretical models of accretion physics and stellar populations. As far as we know, there is little to no work studying the SGWB generated by accretion disks. In this paper, we address this problem. We adopt geometrical units G = c = 1.

II. NUMERICAL SETUP OF ACCRETION DISK

We consider a setup where a BH of mass M, and dimensionless angular momentum χ , is surrounded by an accretion disk. We assume the disk backreacts weakly on the background spacetime, such that for the purposes of matter evolution the spacetime may be assumed to be

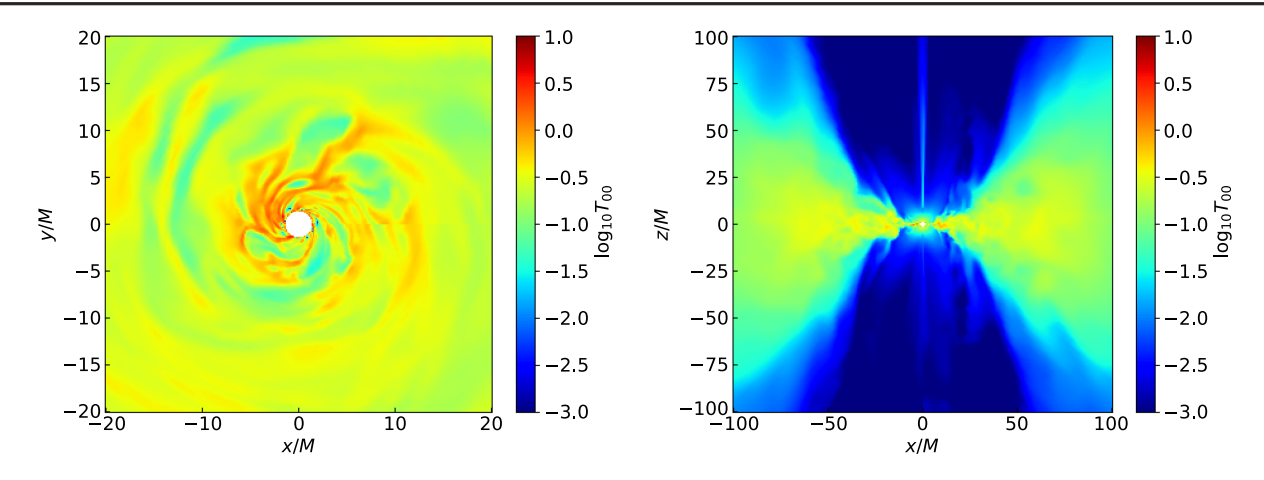


FIG. 1. Initial snapshots of the rest mass density $(T_{00} \equiv \rho)$ of the accretion disk in our simulation, before rescaling. Left panel: cross-sectional cut through the equatorial plane of the disk (z=0). Right panel: two-dimensional cross section of the simulation in the x-z-plane, showing the extended, turbulent disk and low-density funnel regions both above and below the middle plane comprising the jets.

stationary and described by the Kerr metric. The simulations of the matter around the BH are computed using the BHAC code [40,41].

We focus on a Kerr BH with $\chi = 0.94$, adopting spherical Kerr-Schild coordinates with a logarithmic radial coordinate, i.e., $x^1 = \ln r$, focusing resolution in regions closer to the event horizon. The simulation outer boundary is placed at r = 2500M and the inner boundary is well within the event horizon. The grid resolution is $384 \times 192 \times 192$ in x^i (i = 1, 2, 3). The general relativistic magnetohydrodynamics (GRMHD) simulation is initialized with a Fishbone-Moncrief hydrodynamic equilibrium torus profile [42], with $r_{\rm in}=20M$ and $r_{\rm max}=40M$. We employ an ideal gas equation of state with relativistic adiabatic index $\Gamma = 4/3$. The equilibrium torus profile is then suffused with a single weak magnetic field loop, with the radial distribution of the magnetic field profile chosen to ensure sufficient magnetic flux is deposited onto the BH, enabling the magnetically arrested disc state to be reached [43,44]. The magnetorotational instability inside the torus is triggered by applying 2% of a random perturbation to the torus gas pressure. The treatment of very low-density regions and regions of high magnetization is performed in the conventional manner for GRMHD simulations of BHs as follows (e.g., [45]). Floor values are applied to the rest-mass density as $ho_{\mathrm{floor}} =$ $10^{-4}r^{-2}$ and to the gas pressure as $P_{\text{floor}} = (10^{-6}/3)r^{-2\Gamma}$. These ensure that in all grid cells where $\rho \leq \rho_{\mathrm{floor}}$ or $P \le P_{\text{floor}}$, one sets $\rho = \rho_{\text{floor}}$ and $P = P_{\text{floor}}$. We also introduce a ceiling within regions of high magnetization, σ , such that $\sigma_{\text{max}} = 100$ for all grid cells where $\sigma \geq \sigma_{\text{max}}$.

In order to evaluate physical quantities, we begin with the stress-energy tensor of a magnetized perfect fluid:

$$T_{\mu\nu} = (\rho + P + \rho\epsilon + b^2)u_{\mu}u_{\nu} + \left(P + \frac{1}{2}b^2\right)g_{\mu\nu} - b_{\mu}b_{\nu},$$
(1)

where ρ and P represent, respectively, the density and pressure of the fluid, ϵ is the internal energy density, $g_{\mu\nu}$ denotes the metric tensor, u_{μ} is the four velocity of the fluid, and $b^2 \coloneqq b_{\mu}b^{\mu}$, wherein b_{μ} is the magnetic field four vector. We work in Lorentz-Heaviside units, absorbing a factor of $\sqrt{4\pi}$ into the definition of b_{μ} .

After evolving the system for $10^4 M$ to reach a quasistationary state, we extract $T_{\mu\nu}$ with a time step of $\Delta t = 10 M$ for a duration of 2000 M. In order to circumvent the high memory and storage requirements, we uniformly downsample the GRMHD data by a factor of $2(166 \times 96 \times 96)$ when computing $T_{\mu\nu}$, further restricting ourselves to the domain $r_+ < r \le 1000 M$, where $r_+ := M + \sqrt{M^2 - a^2}$ is the event horizon radius of the BH. An initial snapshot of the energy density is shown in Fig. 1, where turbulentlike features are apparent (spiral structures and uneven energy density distribution along the polar directions, indicating the presence of hydrodynamic turbulence).

To evaluate the SGWB from accretion disks, one needs to consider disks with different masses and mass accretion rates. These may be obtained by rescaling the simulation code data, $T_{\mu\nu}^{(\rm code)}$, to physical CGS units, as done in radiative transfer postprocessing [46,47]. The simulation code density scales as $\rho^{(\rm cgs)} = \rho^{\rm unit} \rho^{(\rm code)}$. Introducing the gravitational radius $r_{\rm g} \equiv GM/c^2$, here $\rho^{\rm unit} \equiv \mathcal{M}/r_{\rm g}^3$ and $\mathcal{M} \coloneqq \dot{M}(r_{\rm g}/c)$ is a physical rescaling factor set by the BH's mass accretion rate (\dot{M}) and its mass. The stress-energy tensor of the fluid then scales to physical units by a factor of $c^2 \rho^{\rm unit}$

$$T_{\mu\nu}^{(\text{cgs})} = \left(\frac{\mathcal{M}c^2}{r_{\text{g}}^3}\right) T_{\mu\nu}^{(\text{code})}.$$
 (2)

We parametrize the accretion rate of the central object as

$$\dot{M} = f_{\rm Edd} \dot{M}_{\rm Edd},\tag{3}$$

where the Eddington ratio $f_{\rm Edd}$ is a free parameter that characterizes the accretion rate of the central object in units of the Eddington accretion rate $\dot{M}_{\rm Edd}$ [48]

$$\dot{M}_{\rm Edd} \simeq 2 \times 10^{-8} \left(\frac{M}{M_{\odot}}\right) M_{\odot} \text{ yr}^{-1}.$$
 (4)

III. GRAVITATIONAL RADIATION

Once we have the time-varying stress-energy tensor of the disk, GW emission can be computed by solving Teukolsky's master equation [49,50]. In this approach, the radiative degrees of freedom of the gravitational field at infinity are encoded in a master variable Ψ related to the Newman-Penrose scalar Ψ_4 via $\Psi=(r-ia\cos\theta)^4\Psi_4$ and Ψ_4 is directly related to the GW polarizations via

$$\Psi_4 = \frac{1}{2} \left(\frac{\partial^2 h_+}{\partial t^2} - i \frac{\partial^2 h_\times}{\partial t^2} \right). \tag{5}$$

The Teukolsky master equation is shown in Appendix A. We decompose in azimuthal components Φ_m

$$\Psi(t, r_*, \theta, \tilde{\phi}) = \sum_{m=-\infty}^{\infty} r^3 e^{im\tilde{\phi}} \Phi_m(t, r^*, \theta).$$
 (6)

Here, r_* and $\tilde{\phi}$ are the tortoise coordinates, which are related to Boyer-Lindquist coordinates through

$$\begin{split} r^* &= r + \frac{2Mr_+}{r_+ - r_-} \ln \frac{r - r_+}{2M} - \frac{2Mr_-}{r_+ - r_-} \ln \frac{r - r_-}{2M}, \\ \tilde{\phi} &= \phi + \frac{a}{r_+ - r_-} \ln \frac{r - r_+}{r - r_-}, \end{split} \tag{7}$$

with $r_{\pm} = M \pm \sqrt{M^2 - a^2}$. The source term T in the Teukolsky equation is also decomposed into T_m components. We solve the Teukolsky equation numerically for each m mode in the time domain using the two-step Lax-Wendroff method described in [51–56] with second-order finite differences.

IV. GWS FROM TURBULENTLY EXCITED BHS

The dominant, axially symmetric mode of the GW emitted by the disk is shown in Fig. 2. The turbulent gas flow excites stochastically the BH modes, which is imprinted in the waveform. We find a frequency of order $M\omega \sim 0.42$ (estimated using the number of cycles within the vertical dashed gray lines in the plot) in very good agreement with the quadrupolar $\ell=2$, m=0 quasinormal mode, $M\omega=0.416-i0.0765$ [57]. The "cross" polarization h_{\times} is about an order of magnitude smaller than the "plus" h_{+} reflecting the fact that motion along the radial direction dominates emission. One can expect excitation of higher order modes ($\ell > 2$ modes), but these have larger

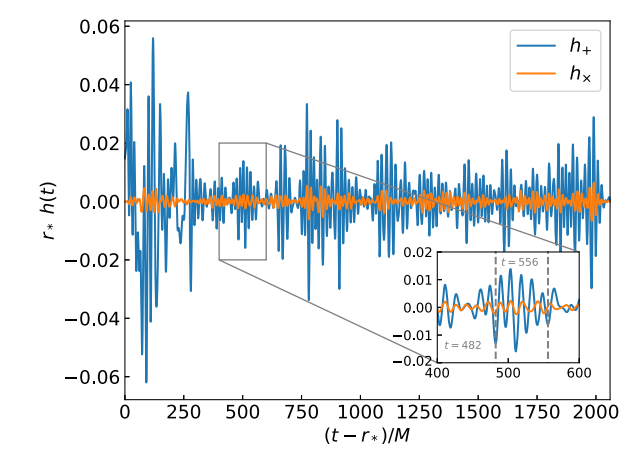


FIG. 2. The m=0 gravitational waveform generated by the accretion disk. The signal is extracted at $r_*^{\rm ext}=500M$. From the time-domain data we estimate the frequency of the signal to be of order $M\omega \sim 0.42$, in good agreement (given our time resolution) with the quadrupolar $\ell=2$, m=0 quasinormal mode, $M\omega=0.416-i0.0765$ [57].

frequencies. To correctly capture these modes we would need prohibitively small (computationally expensive) time steps.

Numerical solutions of the Teukolsky equation can generate unphysical signals—"junk radiation"—as a consequence of arbitrary initial data, which eventually decays in time. We retain the physically meaningful data, for which $t-r_* \gtrsim 300M$, and use it to calculate the energy spectrum of GWs. Figure 3 shows the GW energy spectrum for different m modes. To a good accuracy, the spectrum peaks at the lowest quasinormal frequency of the mode in question [57,58], which is one more piece of evidence that accretion disks are exciting BH ringdown. At higher frequencies, the spectrum decays roughly as a power law. It is tempting to conjecture that the spectrum falls off as $dE/df \sim f^{-5/3}$, corresponding to a Kolmogorov scaling

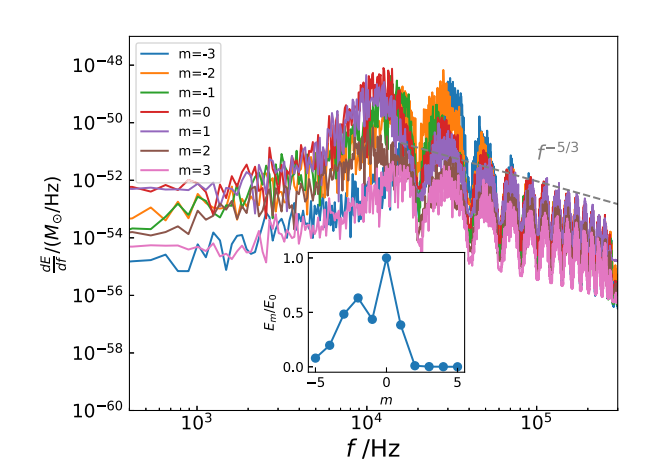


FIG. 3. GW energy spectrum from accretion disk turbulence with $f_{\rm Edd}=1$, for several modes. The BH mass is $M=M_{\odot}$. Inset shows the total energy loss of each m mode, E_m/E_0 .

law [59–61]. The behavior of the energy spectrum at high frequencies (around 10^5 Hz) closely resembles this Kolmogorov scaling, also an indication of the energy cascade. This suggests the possibility that a dissipative region may exist due to the complex internal dynamics within the accretion disk [59–61]. Our results are then consistent with a turbulent accretion disk stochastically exciting the modes of BHs. The energy spectrum exhibits oscillatory behavior at high frequencies due to Nyquist sampling. If we employ higher-order interpolation for the source term when solving the Teukolsky equation, the oscillatory behavior can be mitigated, leading to a power spectrum that scales as $f^{-5/3}$ in the high-frequency band.

The inset of Fig. 3 shows the relative energy carried in each m mode, E_m . The dominant mode is indeed the axial symmetric m=0 and the energy emitted quickly decreases to zero (although, as we said, our simulation is unable to resolve very high ms and these might be underestimated). The quick decay of the power spectrum for higher modes is consistent with Ref. [62], which employs an analytic power series for the turbulent Newtonian potential of the disk.

V. STOCHASTIC GW BACKGROUND

A SGWB is the incoherent superposition of unresolvable GWs. It is characterized by the energy spectrum (energy density per logarithm frequency) normalized by the critical energy:

$$\Omega_{\rm GW}(f) \equiv \frac{1}{\rho_{\rm c}} \frac{\mathrm{d}\rho_{\rm GW}}{\mathrm{d}\ln f}.$$
 (8)

We consider three types of GW-generating disks:

(A) Accretion disks around supermassive BHs (SMBH). Sgr A* observations suggest an accretion rate $10^{-9} \lesssim \dot{M} \lesssim 10^{-7} (M_{\odot}/\mathrm{yr})$, corresponding to a low ratio $f_{\rm Edd} \simeq 10^{-7}$ [63–65]. However, a fraction of the SMBHs in the Universe are known to be actively accreting, i.e., with accretion rates close to the Eddington limit. For example, observations on J0529–4351 find $f_{\rm Edd} \simeq 0.9$ [66], and recently the James Webb Space Telescope has discovered a population of quasars at z=6 [67]. Therefore, we consider three different populations: one with $f_{\rm Edd}=10^{-7}$, one with a uniform distribution $f_{\rm Edd}\in[0,1]$ and super-Eddington accretion [68] with $f_{\rm Edd}\in[0,10]$ for SMBHs at z>3. the energy spectrum of SGWB is evaluated as [69]

$$\Omega_{\rm GW}(f) = \frac{f}{\rho_c} \int dM \, dz \, \frac{dt}{dz} R_{\rm birth}(z, M) \frac{dE_s}{df_s}, \qquad (9)$$

where $R_{\rm birth}(z,M)$ denotes the BH/NS (neutron star)/SMBH formation rate per comoving volume per mass and dE_s/df_s corresponds to the energy spectrum of a single GW event in the source

frame. Here dt/dz is the derivative of the look back time with respect to the redshift, namely $dt/dz = [H_0E(z)(1+z)]^{-1}$, where $E(z) = \sqrt{\Omega_r(1+z)^4 + \Omega_m(1+z)^3 + \Omega_\Lambda}$ $H_0 = 67.4$ km/s/Mpc the Hubble constant at present [70], Ω_r , Ω_m , and Ω_Λ are the density parameters for radiation, matter, and dark energy, respectively. For $R_{\rm birth}$, we adopt the SMBH population model at different z in Ref. [71].

- (B) For an isolated NS (which we take to be described by the Kerr metric [72]) or stellar-origin BH, $f_{\rm Edd}$ is supposed to be $10^{-2} \lesssim f_{\rm Edd} \lesssim 1$ or even beyond the Eddington limit [73–77]. We adopt $f_{\rm Edd} = 1$ here. The SGWB in such a case can also be calculated using Eq. (9) where the computation of $R_{\rm birth}$ for NS and BH can be found in Appendix B.
- (C) Finally, we consider the scenario where the central object is formed from the merger of binary neutron stars (BNSs). Such mergers result in a short-lived accretion disk of subsolar mass [78], corresponding to an accretion rate of $\dot{M} \sim 10^{-2} M_{\odot}/\text{s}$ [39], consistent with numeric simulations [78]. The corresponding SGWB in this case is evaluated as [69]

$$\Omega_{\rm GW}(f) = \frac{f}{\rho_c} \int dM_1 dM_2 dz \frac{dt}{dz} \mathcal{R}(z, M_1, M_2) \frac{dE_s}{df_s},$$
(10)

and we follow [79,80] to obtain the merger rate density,

$$\mathcal{R}(z, M_1, M_2) \propto \int_{t_{\text{min}}}^{t_{\text{max}}} R_{\text{birth}}(t(z) - t_d, M_1)$$
$$\times P_d(t_d) P(M_1) P(M_2) dt_d, \qquad (11)$$

with t(z) the age of the Universe at merger. The function $P_d(t_d) \propto 1/t_d$ is the distribution of delay time with $t_{\rm min} < t_d < t_{\rm max}$. Since the local merger rate of BNS is much larger than the BH-NS binaries and binary BHs [81], we only consider BNSs in the following computation. For BNSs, $t_{\rm min} = 20$ Myr and $t_{\rm max}$ is the Hubble time. The NS mass function has a uniform distribution between $1M_{\odot}$ to $2M_{\odot}$ and we normalize the merger rate density so that the local merger rate is given by $\int \mathcal{R}(z=0,M_1,M_2)dM_1dM_2=1000~{\rm yr}^{-1}~{\rm Gpc}^{-3}$ for BNSs [82,83].

On the other hand, the GRMHD simulation only covers a limited time span, whereas the age of a real BH far exceeds this value. Therefore, we rescale the amplitude of the GW energy spectrum based on the duration time of the GWs, estimated as follows for all three cases

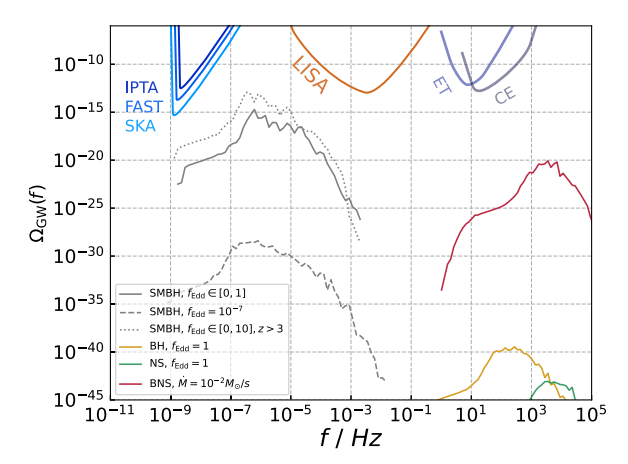


FIG. 4. The SGWB from turbulent accretion disks, compared against the sensitivity curves of GW detectors, including Laser Interferometer Space Antenna (LISA), International Pulsar Timing Array (IPTA), Five-hundred-meter Aperture Spherical radio Telescope (FAST), Square Kilometre Array (SKA), Cosmic Explorer (CE), and Einstein Telescope (ET).

$$\Delta t = \min\left(t_0 - t_{\text{birth}}(z), \frac{M_{\text{disk}}}{\dot{M}}\right),\tag{12}$$

where t_0 is the age of the Universe and $t_{\text{birth}}(z)$ is the formation time of the central object.

The power-law integrated sensitivity curves [84] of various GW detectors are obtained assuming threshold SNR to be SNR = 5 and total observation time of 4 yrs for LISA [85], CE [86], and ET [87], and 30 yrs for IPTA [88], FAST [89], and SKA [90]. We assume two coaligned and colocated identical detectors for CE and ET while for LIGO we use the overlap function [84]. For IPTA/FAST/SKA we assume the pulsars are uniformly distributed in the sky. The number of pulsars and the timing accuracy can be found in Table 5 of [91].

The estimated SGWB, including all modes with $|m| \leq 5$ is shown in Fig. 4. The SGWB generated by the short-lived accretion disks around the remnant of BNSs and the SGWB from isolated NSs/stellar-origin BHs are far below the sensitivity of future ground-based GW detectors. On the other hand, the SGWB from the SMBH population is peaked around 10^{-6} Hz and it could reach $\Omega_{\rm GW} \sim 10^{-15}$ for a uniform distribution $f_{\rm Edd} \in [0,1]$, while it is far below the detection limit if the SMBH population has a small accretion rate $f_{\rm Edd} = 10^{-7}$ as Sgr A*. We also check that the result for $f_{\rm Edd} = 1$ is only slightly larger than $f_{\rm Edd} \in [0,1]$ since the GW emission is dominated by SMBHs with large accretion rate.

Although the GRMHD simulations are traditionally employed for modeling accretion disks around SMBHs, we extend their application to systems involving stellar-origin BHs and NSs. It is worth noting that the direct application of the GRMHD simulations to stellar mass objects may introduce uncertainties due to different physical conditions, such as differences in magnetic field configurations.

VI. DISCUSSION

In this paper, we explore the contribution of turbulence in accretion disks around BHs and NSs to the emission of GWs, in particular to stochastic backgrounds. Feeding GRMHD simulations as a source term to the Teukolsky equation, we have quantified the GW energy spectrum from these systems. The waveform and energy spectrum analysis indicate that turbulent flows in accretion disks stochastically excite the quasinormal modes of the BHs [92,93]. The energy spectrum shows a power-law decay, which scales as the expected Kolmogorov decay $dE/df \sim f^{-5/3}$ for a turbulent system. Our results indicate that the SGWB from accretion disks around NSs, stellar-origin BHs and the remnants from the merger of BNSs are undetectable due to their low amplitudes. Note that Eq. (10) implies that we assume all the BNS merger lead to short-lived accretion disks. However, the SGWB is still far below the sensitivity curves, indicating case 3 is of low interest despite of their large accretion rates. We neglect differences between QNMs of NSs and those of BHs [94]. However, as the SGWB from NSs and BNSs are far below the sensitivity of future detectors, this simplification will most likely not affect our overall conclusions. On the other hand, accretion disks around SMBHs could generate an SGWB at $\Omega_{GW} \sim 10^{-15}$ in the microhertz frequencies. We also explored the astrophysical implications of super-Eddington accreting systems at z > 3. The resulting $\Omega_{\rm GW} \sim$ 10⁻¹⁴ might be an interesting prospect for future GW detectors in this frequency band. Additionally, our findings motivate multimessenger studies that link the GW signals from accretion disk-induced mode excitation to electromagnetic observations of accretion disks around compact objects. This could provide a unique window into the dynamics of accretion flows and the environments of SMBHs.

ACKNOWLEDGMENTS

We acknowledge the support by VILLUM Foundation (Grant No. VIL37766) and the DNRF Chair program (Grant No. DNRF162) by the Danish National Research Foundation. V.C. is a Villum Investigator and a DNRF Chair. C. Y. and V.C. acknowledge financial support provided under the European Union's H2020 ERC Advanced Grant "Black holes: gravitational engines of discovery" Grant Agreement No. Gravitas-101052587. Z. Y. is supported by a UK Research and Innovation (UKRI) Stephen Hawking Fellowship. This project has received funding from the European Union's Horizon 2020 research and innovation programme under the Marie Sklodowska-Curie Grants Agreement No. 101007855 and No. 101131233.

Views and opinions expressed are however those of the author only and do not necessarily reflect those of the European Union or the European Research Council. Neither the European Union nor the granting authority can be held responsible for them.

APPENDIX A: THE TEUKOLSKY EQUATION

The Teukolsky equation expressed in Boyer-Lindquist coordinates reads

$$\begin{split} &\Delta^2 \partial_r (\Delta^{-1} \partial_r \Psi) - \left[\frac{(r^2 + a^2)^2}{\Delta} - a^2 \sin^2 \theta \right] \partial_{tt} \Psi + 4 \left[r - \frac{M(r^2 - a^2)}{\Delta} + ia \cos \theta \right] \partial_t \Psi + \frac{1}{\sin \theta} \partial_{\theta} (\sin \theta \partial_{\theta} \Psi) \\ &+ \left[\frac{1}{\sin^2 \theta} - \frac{a^2}{\Delta} \right] \partial_{\phi \phi} \Psi - 4 \left[\frac{a(r - M)}{\Delta} + \frac{i \cos \theta}{\sin^2 \theta} \right] \partial_{\phi} \Psi - (4 \cot^2 \theta + 2) \Psi - \frac{4Mar}{\Delta} \partial_{t\phi} \Psi = -4\pi (r^2 + a^2 \cos^2 \theta) T, \end{split} \tag{A1}$$

where $a = M\chi$ is the BH angular momentum, $\Delta = r^2 - 2Mr + a^2$, and T is a source term computed from the stress-energy tensor. In Boyer-Lindquist coordinates the tetrad vectors are defined as

$$n^{\mu} = \left(\frac{\rho\bar{\rho}(r^2 + a^2)}{2}, -\frac{\Delta\rho\bar{\rho}}{2}, 0, \frac{a\rho\bar{\rho}}{2}\right), \qquad \bar{m}^{\mu} = \frac{(-ia\,\sin\theta, 0, 1, -i\,\cos\theta)}{\sqrt{2}(r - ia\,\cos\theta)},\tag{A2}$$

where $\rho^{-1} = -(r - ia \cos \theta)$ and a bar represents the complex conjugate. The Newman-Penrose operators are

$$\tilde{\Delta} = n^{\mu} \frac{\mathrm{d}}{\mathrm{d}x^{\mu}}, \qquad \tilde{\delta} = \bar{m}^{\mu} \frac{\mathrm{d}}{\mathrm{d}x^{\mu}}.$$
 (A3)

The source term of the Teukolsky equation can be expressed in a generic form such that

$$T = 2(r - ia \cos \theta)^{4} T_{4},$$

$$T_{4} = (\tilde{\Delta} + 3\gamma - \bar{\gamma} + 4\mu + \bar{\mu})(\tilde{\Delta} + 2\gamma - 2\bar{\gamma} + \bar{\mu})T_{\bar{m}\bar{m}} - (\tilde{\Delta} + 3\gamma - \bar{\gamma} + 4\mu + \bar{\mu})(\bar{\delta} - 2\bar{\tau} + 2\alpha)T_{n\bar{m}} + (\bar{\delta} - \bar{\tau} + \bar{\beta} + 3\alpha + 4\pi)(\bar{\delta} - \bar{\tau} + 2\bar{\beta} + 2\alpha)T_{nn} - (\bar{\delta} - \bar{\tau} + \bar{\beta} + 4\pi)(\tilde{\Delta} + 2\gamma + 2\bar{\mu})T_{n\bar{m}}.$$
(A4)

The projected stress-energy tensor is defined as $T_{nn} = n^{\mu} n^{\nu} T_{\mu\nu}$, $T_{n\bar{m}} = n^{\mu} \bar{m}^{\nu} T_{\mu\nu}$ and $T_{\bar{m}\bar{m}} = \bar{m}^{\mu} \bar{m}^{\nu} T_{\mu\nu}$. The Newmann-Penrose scalars are given by (see, e.g., [95])

$$\rho = -\frac{1}{\bar{\Gamma}}, \qquad \beta = \frac{\cot \theta}{2^{3/2} \Gamma}, \qquad \pi = \frac{i a \sin \theta}{2^{1/2} \bar{\Gamma}^2},$$

$$\tau = -\frac{i a \sin \theta}{2^{1/2} \Gamma \bar{\Gamma}}, \qquad \mu = -\frac{\Delta}{2 \Gamma \bar{\Gamma}^2}, \qquad \gamma = \mu + \frac{r - M}{2 \Gamma \bar{\Gamma}},$$

$$\alpha = \pi - \bar{\beta}, \qquad \Psi_2 = -\frac{M}{\bar{\Gamma}^3}, \qquad (A5)$$

with $\Gamma = r + ia \cos \theta$.

BHAC uses Kerr-Schild coordinates, with which the tetrad vectors become

$$n^{\mu} = \left[\frac{1}{2\Sigma}, -\frac{1}{2\Sigma}, 0, 0 \right],\tag{A6}$$

where $\Sigma = r^2 + a^2 \cos^2 \theta$ while \bar{m} remains unchanged. The Newmann-Penrose scalars become

$$\epsilon = r - M, \qquad \gamma = \mu = -\frac{1}{2} \frac{r + ia \cos \theta}{\Sigma^2}, \qquad \rho = -(r + ia \cos \theta) \frac{\triangle}{\Sigma}.$$
 (A7)

The rest of the quantities remain unchanged. Finally, the Newman-Penrose operator becomes

$$\tilde{\Delta} = n^{\mu} \frac{\mathrm{d}}{\mathrm{d}x^{\mu}} = \frac{1}{2\Sigma} \left(\frac{\mathrm{d}}{\mathrm{d}t} - \frac{\mathrm{d}}{\mathrm{d}r} \right),\tag{A8}$$

while $\tilde{\delta}$ remains unchanged.

APPENDIX B: BLACK HOLE/NEUTRON STAR FORMATION RATE

We follow Ref. [96] to compute the BH/NS formation rate, which takes the form

$$R_{\rm birth} = \int \psi[t-\tau(M_*)]\phi(M_*)\delta(M_*-g_{\rm rem}^{-1}(M,z)){\rm d}M_*, \eqno(B1)$$

where M_* is the progenitor star mass and $\psi(z)$ is the star formation rate, which takes the form

$$\psi(z) = \nu \frac{a \exp[b(z - z_m)]}{a - b + b \exp[a(z - z_m)]},$$
 (B2)

and the parameters are given by $\nu=0.178M_{\odot}~\rm yr^{-1}~Mpc^{-3}$, $z_m=2.00, a=2.37, b=1.80~\rm [97]$. The lifetime of the progenitor star in Eq. (B1), $\tau(M_*)$ can be computed as [98]

$$\log_{10}\tau(M_*) = 9.785 - 3.759x + 1.413x^2 - 0.186x^3, \quad (B3)$$

with $x = \log_{10}(M/M_{\odot})$. The initial mass function is given by $\phi(M_*) \propto M_*^{-2.35}$ for BHs [99] and we consider a uniform distribution between $1M_{\odot}$ and $2M_{\odot}$ for NSs. The mass of a BH/NS remnant is related to the mass of the progenitor star by $M = g_{\rm rem}(M_*, z)$ and can be evaluated as [100]

$$M = \begin{cases} 1.28, & M_* < 11M_{\odot} \\ 1.1 + 0.2e^{(M_*-11.0)/4.0} - (2.0 + Z(z)/Z_{\odot})e^{0.4(M_*-26.0)}, & 11M_{\odot} \leq M_* < 30M_{\odot} \\ \min{(33.35 + (4.75 + 1.25Z(z)/Z_{\odot})(M_* - 34)}, & M_* - \sqrt{Z(z)/Z_{\odot}}(1.3M_* - 18.35)), & 30M_{\odot} \leq M_* < 50M_{\odot}, \\ 1.8 + 0.04 \times (90 - M_*), & 50M_{\odot} \leq M_* < 90M_{\odot} \\ 1.8 + \log_{10}(M_* - 89), & M_* \geq 90M_{\odot} \end{cases}$$

$$(B4)$$

where $Z_{\odot} = 0.0196$ is metallicity of the Sun [101]. The metallicity of the progenitor star as a function of the redshift is given by [102]

$$\log_{10} Z(z) = 0.5 + \log_{10} \left(\frac{0.01387}{\rho_b} \int_z^{20} \frac{97.8 \times 10^{10} \psi(z')}{H_0 E(z') (1+z')} dz' \right), \tag{B5}$$

where $\rho_b = 6.1 \times 10^9 M_{\odot} \,\mathrm{Mpc^{-3}}$ and $E(z) = \sqrt{\Omega_r (1+z)^4 + \Omega_m (1+z)^3 + \Omega_{\Lambda}}$.

^[1] B. P. Abbott *et al.* (LIGO Scientific and Virgo Collaborations), Binary black hole mergers in the first Advanced LIGO observing run, Phys. Rev. X **6**, 041015 (2016); **8**, 039903(E) (2018).

^[2] R. Abbott *et al.* (LIGO Scientific, VIRGO, and KAGRA Collaborations), GWTC-3: Compact binary coalescences observed by LIGO and Virgo during the second part of the third observing run, Phys. Rev. X 13, 041039 (2023).

^[3] Nicolás Yunes and Xavier Siemens, Gravitational-wave tests of general relativity with ground-based detectors and pulsar timing-arrays, Living Rev. Relativity **16**, 9 (2013).

^[4] Emanuele Berti *et al.*, Testing general relativity with present and future astrophysical observations, Classical Quantum Gravity **32**, 243001 (2015).

^[5] Leor Barack *et al.*, Black holes, gravitational waves and fundamental physics: A roadmap, Classical Quantum Gravity **36**, 143001 (2019).

^[6] Vitor Cardoso and Paolo Pani, Testing the nature of dark compact objects: A status report, Living Rev. Relativity 22, 4 (2019).

^[7] Edward Witten, Cosmic separation of phases, Phys. Rev. D **30**, 272 (1984).

^[8] Arthur Kosowsky, Michael S. Turner, and Richard Watkins, Gravitational waves from first order cosmological phase transitions, Phys. Rev. Lett. **69**, 2026 (1992).

^[9] Arthur Kosowsky, Michael S. Turner, and Richard Watkins, Gravitational radiation from colliding vacuum bubbles, Phys. Rev. D 45, 4514 (1992).

- [10] Marc Kamionkowski, Arthur Kosowsky, and Michael S. Turner, Gravitational radiation from first order phase transitions, Phys. Rev. D 49, 2837 (1994).
- [11] Zaven Arzoumanian *et al.* (NANOGrav Collaboration), Searching for gravitational waves from cosmological phase transitions with the NANOGrav 12.5-year dataset, Phys. Rev. Lett. **127**, 251302 (2021).
- [12] Xiao Xue et al., Constraining cosmological phase transitions with the parkes pulsar timing array, Phys. Rev. Lett. 127, 251303 (2021).
- [13] Alba Romero, Katarina Martinovic, Thomas A. Callister, Huai-Ke Guo, Mario Martínez, Mairi Sakellariadou, Feng-Wei Yang, and Yue Zhao, Implications for first-order cosmological phase transitions from the third LIGO-Virgo observing run, Phys. Rev. Lett. 126, 151301 (2021).
- [14] Yang Jiang and Qing-Guo Huang, Constraining the gravitational-wave spectrum from cosmological first-order phase transitions using data from LIGO-Virgo first three observing runs, J. Cosmol. Astropart, Phys. 06 (2023) 053.
- [15] Misao Sasaki, Teruaki Suyama, Takahiro Tanaka, and Shuichiro Yokoyama, Primordial black hole scenario for the gravitational-wave event GW150914, Phys. Rev. Lett. 117, 061101 (2016); 121, 059901(E) (2018).
- [16] Chen Yuan and Qing-Guo Huang, A topic review on probing primordial black hole dark matter with scalar induced gravitational waves, iScience **24**, 102860 (2021).
- [17] Zu-Cheng Chen, Chen Yuan, and Qing-Guo Huang, Pulsar timing array constraints on primordial black holes with NANOGrav 11-year dataset, Phys. Rev. Lett. **124**, 251101 (2020).
- [18] Chen Yuan, Yang Jiang, and Qing-Guo Huang, Constraints on an ultralight scalar boson from Advanced LIGO and Advanced Virgo's first three observing runs using the stochastic gravitational-wave background, Phys. Rev. D 106, 023020 (2022).
- [19] Leo Tsukada, Thomas Callister, Andrew Matas, and Patrick Meyers, First search for a stochastic gravitational-wave background from ultralight bosons, Phys. Rev. D 99, 103015 (2019).
- [20] Leo Tsukada, Richard Brito, William E. East, and Nils Siemonsen, Modeling and searching for a stochastic gravitational-wave background from ultralight vector bosons, Phys. Rev. D 103, 083005 (2021).
- [21] Chen Yuan, Richard Brito, and Vitor Cardoso, Probing ultralight dark matter with future ground-based gravitational-wave detectors, Phys. Rev. D **104**, 044011 (2021).
- [22] John Preskill, Mark B. Wise, and Frank Wilczek, Cosmology of the invisible axion, Phys. Lett. **120B**, 127 (1983).
- [23] L. F. Abbott and P. Sikivie, A cosmological bound on the invisible axion, Phys. Lett. 120B, 133 (1983).
- [24] Michael Dine and Willy Fischler, The not so harmless axion, Phys. Lett. **120B**, 137 (1983).
- [25] Asimina Arvanitaki, Savas Dimopoulos, Sergei Dubovsky, Nemanja Kaloper, and John March-Russell, String axiverse, Phys. Rev. D 81, 123530 (2010).
- [26] Asimina Arvanitaki and Sergei Dubovsky, Exploring the string axiverse with precision black hole physics, Phys. Rev. D 83, 044026 (2011).
- [27] Rouven Essig *et al.*, Working group report: New light weakly coupled particles, in Community Summer Study

- 2013: Snowmass on the Mississippi(2013), arXiv: 1311.0029.
- [28] Richard Brito, Vitor Cardoso, and Paolo Pani, Superradiance: New frontiers in black hole physics, Lect. Notes Phys. 906, 1 (2015).
- [29] David J. E. Marsh, Axion cosmology, Phys. Rep. 643, 1 (2016).
- [30] Lam Hui, Jeremiah P. Ostriker, Scott Tremaine, and Edward Witten, Ultralight scalars as cosmological dark matter, Phys. Rev. D 95, 043541 (2017).
- [31] Lorenzo Annulli, Vitor Cardoso, and Rodrigo Vicente, Response of ultralight dark matter to supermassive black holes and binaries, Phys. Rev. D 102, 063022 (2020).
- [32] Francesca Chadha-Day, John Ellis, and David J. E. Marsh, Axion dark matter: What is it and why now?, Sci. Adv. 8, abj3618 (2022).
- [33] Steven A. Balbus and John F. Hawley, A powerful local shear instability in weakly magnetized disks. I. Linear analysis, Astrophys. J. **376**, 214 (1991).
- [34] Steven A. Balbus and John F. Hawley, Instability, turbulence, and enhanced transport in accretion disks, Rev. Mod. Phys. **70**, 1 (1998).
- [35] P. Goldreich and D. A. Keeley, Solar seismology. I. The stability of the solar p-modes, Astrophys. J. 211, 934 (1977).
- [36] P. Goldreich and D. A. Keeley, Solar seismology. II. The stochastic excitation of the solar p-modes by turbulent convection, Astrophys. J. 212, 243 (1977).
- [37] Jorgen Christensen-Dalsgaard, Helioseismology, Rev. Mod. Phys. 74, 1073 (2003).
- [38] Rafael Angel Araya-Gochez, Gravitational waves from hyper-accretion onto nascent black holes, Mon. Not. R. Astron. Soc. 355, 336 (2004).
- [39] Ore Gottlieb, Amir Levinson, and Yuri Levin, In LIGO's sight? Vigorous coherent gravitational waves from cooled collapsar disks, Astrophys. J. Lett. 972, L4 (2024).
- [40] Oliver Porth, Hector Olivares, Yosuke Mizuno, Ziri Younsi, Luciano Rezzolla, Monika Moscibrodzka, Heino Falcke, and Michael Kramer, The black hole accretion code, Comput. Astrophys. Cosmol. **4**, 1 (2017).
- [41] Hector Olivares, Oliver Porth, Jordy Davelaar, Elias R. Most, Christian M. Fromm, Yosuke Mizuno, Ziri Younsi, and Luciano Rezzolla, Constrained transport and adaptive mesh refinement in the black hole accretion code, Astron. Astrophys. 629, A61 (2019).
- [42] L. G. Fishbone and V. Moncrief, Relativistic fluid disks in orbit around Kerr black holes, Astrophys. J. **207**, 962 (1976).
- [43] Ramesh Narayan, Igor V. Igumenshchev, and Marek A. Abramowicz, Magnetically arrested disk: An energetically efficient accretion flow, Publ. Astron. Soc. Jpn. 55, L69 (2003).
- [44] Alexander Tchekhovskoy, Ramesh Narayan, and Jonathan C. McKinney, Efficient generation of jets from magnetically arrested accretion on a rapidly spinning black hole, Mon. Not. R. Astron. Soc. 418, L79 (2011).
- [45] Yosuke Mizuno, Christian M. Fromm, Ziri Younsi, Oliver Porth, Hector Olivares, and Luciano Rezzolla, Comparison of the ion-to-electron temperature ratio prescription: GRMHD simulations with electron thermodynamics, Mon. Not. R. Astron. Soc. **506**, 741 (2021).

- [46] Z. Younsi, K. Wu, and S. V. Fuerst, General relativistic radiative transfer: Formulation and emission from structured tori around black holes, Astron. Astrophys. 545, A13 (2012).
- [47] Ziri Younsi, Dimitrios Psaltis, and Feryal Özel, Black hole images as tests of general relativity: Effects of spacetime geometry, Astrophys. J. 942, 47 (2023).
- [48] Feng Yuan and Ramesh Narayan, Hot accretion flows around black holes, Annu. Rev. Astron. Astrophys. 52, 529 (2014).
- [49] S. A. Teukolsky, Rotating black holes—separable wave equations for gravitational and electromagnetic perturbations, Phys. Rev. Lett. 29, 1114 (1972).
- [50] Saul A. Teukolsky, Perturbations of a rotating black hole. I. Fundamental equations for gravitational electromagnetic and neutrino field perturbations, Astrophys. J. 185, 635 (1973).
- [51] William Krivan, Pablo Laguna, Philippos Papadopoulos, and Nils Andersson, Dynamics of perturbations of rotating black holes, Phys. Rev. D 56, 3395 (1997).
- [52] Ramon Lopez-Aleman, Gaurav Khanna, and Jorge Pullin, Perturbative evolution of particle orbits around Kerr black holes: Time domain calculation, Classical Quantum Gravity 20, 3259 (2003).
- [53] Enrique Pazos-Avalos and Carlos O. Lousto, Numerical integration of the Teukolsky equation in the time domain, Phys. Rev. D 72, 084022 (2005).
- [54] Pranesh A. Sundararajan, Gaurav Khanna, and Scott A. Hughes, Towards adiabatic waveforms for inspiral into Kerr black holes. I. A new model of the source for the time domain perturbation equation, Phys. Rev. D 76, 104005 (2007).
- [55] Vitor Cardoso, Francisco Duque, and Gaurav Khanna, Gravitational tuning forks and hierarchical triple systems, Phys. Rev. D 103, L081501 (2021).
- [56] Vitor Cardoso, Francisco Duque, and Arianna Foschi, Light ring and the appearance of matter accreted by black holes, Phys. Rev. D **103**, 104044 (2021).
- [57] Emanuele Berti, Vitor Cardoso, and Clifford M. Will, On gravitational-wave spectroscopy of massive black holes with the space interferometer LISA, Phys. Rev. D 73, 064030 (2006).
- [58] Emanuele Berti, Vitor Cardoso, and Andrei O. Starinets, Quasinormal modes of black holes and black branes, Classical Quantum Gravity **26**, 163001 (2009).
- [59] A. N. Kolmogorov, The local structure of turbulence in incompressible viscous fluid for very large Reynolds number, Dokl. Akad. Nauk SSSR 30, 299 (1941); reprinted in Proc. R. Soc. A 434, 9 (1991).
- [60] A. N. Kolmogorov, On degeneration (decay) of isotropic turbulence in an incompressible viscous liquid, Dokl. Akad. Nauk SSSR 31, 538 (1941).
- [61] A. N. Kolmogorov, Dissipation of energy in locally isotropic turbulence, Dokl. Akad. Nauk SSSR 32, 16 (1941); reprinted in Proc. R. Soc. A 434, 15 (1991).
- [62] Yinhao Wu, Yi-Xian Chen, and Douglas N. C. Lin, Chaotic Type I migration in turbulent discs, Mon. Not. R. Astron. Soc. 528, L127 (2023).
- [63] D. K. Aitken, J. Greaves, Antonio Chrysostomou, T. Jenness, W. Holland, J. H. Hough, D. Pierce-Price, and J. Richer, Detection of polarized millimeter

- and submillimeter emission from Sagittarius A*, Astrophys. J. **534**, L173 (2000).
- [64] Geoffrey C. Bower, Melvyn C. H. Wright, Heino Falcke, and Donald C. Backer, Interferometric detection of linear polarization from Sagittarius A* at 230 GHz, Astrophys. J. **588**, 331 (2003).
- [65] D. P. Marrone, J. M. Moran, J. H. Zhao, and R. Rao, An unambiguous detection of faraday rotation in Sagittarius A*, Astrophys. J. Lett. 654, L57 (2006).
- [66] Christian Wolf, Samuel Lai, Christopher A. Onken, Neelesh Amrutha, Fuyan Bian, Wei Jeat Hon, Patrick Tisserand, and Rachel L. Webster, The accretion of a solar mass per day by a 17-billion solar mass black hole, Nat. Astron. 8, 520 (2024).
- [67] Jinyi Yang *et al.*, Probing early supermassive black hole growth and quasar evolution with near-infrared spectroscopy of 37 reionization-era quasars at $6.3 < z \le 7.64$, Astrophys. J. **923**, 262 (2021).
- [68] Hyewon Suh *et al.*, Feeding hidden monsters: A supereddington accreting black hole ~1.5 Gyr after the big bang, arXiv:2405.05333.
- [69] E. S. Phinney, A practical theorem on gravitational wave backgrounds, arXiv:astro-ph/0108028.
- [70] N. Aghanim *et al.* (Planck Collaboration), Planck 2018 results. VI. Cosmological parameters, Astron. Astrophys. **641**, A6 (2020); **652**, C4(E) (2021).
- [71] Brandon C. Kelly, Marianne Vestergaard, Xiaohui Fan, Philip Hopkins, Lars Hernquist, and Aneta Siemiginowska, Constraints on black hole growth, quasar lifetimes, and eddington ratio distributions from the SDSS broad line quasar black hole mass function, Astrophys. J. 719, 1315 (2010).
- [72] Francisco Frutos-Alfaro, Approximate spacetime for neutron stars, Gen. Relativ. Gravit. 51, 46 (2019).
- [73] M. Bachetti *et al.*, An ultraluminous x-ray source powered by an accreting neutron star, Nature (London) 514, 202 (2014).
- [74] G. L. Israel *et al.*, An accreting pulsar with extreme properties drives an ultraluminous x-ray source in NGC 5907, Science 355, 817 (2017).
- [75] F. Fürst, D. J. Walton, D. Stern, M. Bachetti, D. Barret, M. Brightman, F. A. Harrison, and V. Rana, Spectral changes in the hyperluminous pulsar in NGC 5907 as a function of super-orbital phase, Astrophys. J. 834, 77 (2017).
- [76] M. Brightman et al., Breaking the limit: Super-Eddington accretion onto black holes and neutron stars, arXiv: 1903.06844.
- [77] Shogo Yoshioka, Shin Mineshige, Ken Ohsuga, Tomohisa Kawashima, and Takaaki Kitaki, Radiation and outflow properties of super-Eddington accretion flows around various mass classes of black holes: Dependence on the accretion rates, arXiv:2407.15927.
- [78] Kenta Kiuchi, Sho Fujibayashi, Kota Hayashi, Koutarou Kyutoku, Yuichiro Sekiguchi, and Masaru Shibata, Self-consistent picture of the mass ejection from a one second long binary neutron star merger leaving a short-lived remnant in a general-relativistic neutrino-radiation magnetohydrodynamic simulation, Phys. Rev. Lett. 131, 011401 (2023).
- [79] B. P. Abbott *et al.* (LIGO Scientific and Virgo Collaborations), GW150914: Implications for the stochastic

- gravitational wave background from binary black holes, Phys. Rev. Lett. **116**, 131102 (2016).
- [80] Benjamin P. Abbott et al. (LIGO Scientific and Virgo Collaborations), GW170817: Implications for the stochastic gravitational-wave background from compact binary coalescences, Phys. Rev. Lett. 120, 091101 (2018).
- [81] R. Abbott et al. (KAGRA, VIRGO, and LIGO Scientific Collaborations), Population of merging compact binaries inferred using gravitational waves through GWTC-3, Phys. Rev. X 13, 011048 (2023).
- [82] R. Abbott *et al.* (LIGO Scientific and Virgo Collaborations), Population properties of compact objects from the second LIGO-Virgo gravitational-wave transient catalog, Astrophys. J. Lett. **913**, L7 (2021).
- [83] Maryam Aghaei Abchouyeh, Maurice H. P. M. van Putten, and Lorenzo Amati, Observational prospects of double neutron star mergers and their multimessenger afterglows: LIGO discovery power, event rates, and diversity, Astrophys. J. 952, 157 (2023).
- [84] Eric Thrane and Joseph D. Romano, Sensitivity curves for searches for gravitational-wave backgrounds, Phys. Rev. D 88, 124032 (2013).
- [85] Pau Amaro-Seoane et al. (LISA Collaboration), Laser interferometer space antenna, arXiv:1702.00786.
- [86] Benjamin P. Abbott et al. (LIGO Scientific Collaboration), Exploring the sensitivity of next generation gravitational wave detectors, Classical Quantum Gravity 34, 044001 (2017).
- [87] M. Punturo *et al.*, The Einstein telescope: A third-generation gravitational wave observatory, Classical Quantum Gravity 27, 194002 (2010).
- [88] G. Hobbs *et al.*, The international pulsar timing array project: Using pulsars as a gravitational wave detector, Classical Quantum Gravity **27**, 084013 (2010).
- [89] Rendong Nan, Di Li, Chengjin Jin, Qiming Wang, Lichun Zhu, Wenbai Zhu, Haiyan Zhang, Youling Yue, and Lei Qian, The five-hundred-meter aperture spherical radio telescope (FAST) project, Int. J. Mod. Phys. D 20, 989 (2011).
- [90] Michael Kramer and Ben Stappers, Pulsar science with the SKA, arXiv:1507.04423.
- [91] Kazuaki Kuroda, Wei-Tou Ni, and Wei-Ping Pan, Gravitational waves: Classification, methods of detection,

- sensitivities, and sources, Int. J. Mod. Phys. D **24**, 1530031 (2015).
- [92] V. Ferrari, L. Gualtieri, and L. Rezzolla, A hybrid approach to black hole perturbations from extended matter sources, Phys. Rev. D 73, 124028 (2006).
- [93] A. Nagar, O. Zanotti, J. A. Font, and L. Rezzolla, On the accretion-induced QNM excitation of a Schwarzschild black hole, Phys. Rev. D 75, 044016 (2007).
- [94] B. F. Schutz, Asteroseismology of neutron stars and black holes, J. Phys. Conf. Ser. 118, 012005 (2008).
- [95] Nicholas Loutrel, Justin L. Ripley, Elena Giorgi, and Frans Pretorius, Second order perturbations of Kerr black holes: Reconstruction of the metric, Phys. Rev. D 103, 104017 (2021).
- [96] Irina Dvorkin, Elisabeth Vangioni, Joseph Silk, Jean-Philippe Uzan, and Keith A. Olive, Metallicity-constrained merger rates of binary black holes and the stochastic gravitational wave background, Mon. Not. R. Astron. Soc. 461, 3877 (2016).
- [97] E. Vangioni, K. A. Olive, T. Prestegard, J. Silk, P. Petitjean, and V. Mandic, The impact of star formation and gammaray burst rates at high redshift on cosmic chemical evolution and reionization, Mon. Not. R. Astron. Soc. 447, 2575 (2015).
- [98] Daniel Schaerer, On the properties of massive population III stars and metal-free stellar populations, Astron. Astrophys. **382**, 28 (2002).
- [99] Edwin E. Salpeter, The luminosity function and stellar evolution, Astrophys. J. 121, 161 (1955).
- [100] Chris L. Fryer, Krzysztof Belczynski, Grzegorz Wiktorowicz, Michal Dominik, Vicky Kalogera, and Daniel E. Holz, Compact remnant mass function: Dependence on the explosion mechanism and metallicity, Astrophys. J. 749, 91 (2012).
- [101] Sunny Vagnozzi, New solar metallicity measurements, Atoms 7, 41 (2019).
- [102] Krzysztof Belczynski, Daniel E. Holz, Tomasz Bulik, and Richard O'Shaughnessy, The first gravitational-wave source from the isolated evolution of two 40-100 solar mass range, Nature (London) 534, 512 (2016).